Renewable Energy 168 (2021) 45–56

Contents lists available at ScienceDirect

Renewable Energy

journal homepage: www.elsevier.com/locate/renene

Optimal combination of bioenergy and solar photovoltaic for renewable energy production on abandoned cropland

Malene Eldegard Leirpoll *, Jan Sandstad Næss , Otavio Cavalett , Martin Dorber , Xiangping Hu , Francesco Cherubini

Department of Energy and Process Engineering, Industrial Ecology Programme, Norwegian University of Science and Technology (NTNU), Høgskoleringen 1, 7491, Trondheim, Norway

ARTICLE INFO

Article history:
Received 6 September 2020
Received in revised form
9 November 2020
Accepted 30 November 2020
Available online 4 December 2020

Keywords:
Bioenergy
Solar energy
Land use
Renewable energy
Abandoned cropland

ABSTRACT

Ambitious climate change mitigation scenarios require large-scale deployment of bioenergy and solar photovoltaics. Utilizing recently abandoned cropland for renewable energy production is a promising option for energy supply while reducing competition for land and food security. However, the magnitude of abandoned cropland and its potential for renewable energy production is still unclear. Here, we mapped recently abandoned croplands at a global level and assessed the site-specific primary energy potentials for bioenergy and solar photovoltaics considering local climatic conditions, energy yields, and socio-economic feasibility constraints to identify optimal land use for renewable energy production. Of the 83 Mha of the identified abandoned cropland between 1992 and 2015, 68% of the area presented higher development potentials for the establishment of solar photovoltaic compared to dedicated bioenergy crops. In total, 125 EJ/year of primary energy can be produced with this optimal land management, of which 114 EJ/year is from solar photovoltaic and 11 EJ/year is from bioenergy. This figure corresponds to 33–50% of the projected median renewable energy demand in 2050 across the 1.5 °C stabilization scenarios. Mapping the suitability of renewable energy sources across different local, environmental, and socio-economic constraints will help identify the best implementation options for future energy systems transformation.

1. Introduction

The continuing rise in greenhouse gases (GHG) emissions presents a significant challenge for limiting warming to well below 2 °C relative to the pre-industrial era [1]. According to the International Energy Agency (IEA), the energy production by renewable energy sources experienced a record-high increase in 2019, both in terms of the fastest rate of growth and the largest absolute growth [2]. Despite these positive developments in the renewable energy sector, the transformation of global energy systems is still far from the levels required to meet the objectives of the Paris Agreement and deployment of renewable energy solutions must accelerate substantially [3].

The different Shared Socio-economic Pathways (SSP) expect higher future demands for second-generation bioenergy crops and increased energy production from renewable energy sources, especially solar photovoltaic (PV) [4,5]. Of those projections that can reach the 1.5 °C target by 2100, the annual primary energy needed from biomass and PV is in the range of 87–453 EJ and 54–396 EJ, respectively [5,6]. For providing such large amounts of primary energy from bioenergy and PV, different extents of land resources are required, which may conflict with other land uses, such as biodiversity conservation, and food security [7,8]. In order to distinguish the most appropriate solutions across different locations and socio-economic contexts, robust land and energy management planning is vital [9,10]. Mapping land that would be suitable for establishing renewable energy infrastructure under a range of environmental and socio-economic criteria is an essential tool for a sustainable energy transition [11,12]. Utilizing areas of recently abandoned cropland for the establishment of renewable energy infrastructure is a promising option for energy supply while reducing potential competition for land and its potential impacts on biodiversity and food security [13–15]. Conversion of abandoned cropland to active forms of energy supply is usually considered a near-term no-regrets opportunity to gradually achieve

* Corresponding author. Tromsøgata 17, 0565, OSLO, Norway.
E-mail address: malene@villenergi.no (M.E. Leirpoll).

https://doi.org/10.1016/j.renene.2020.11.159

large-scale renewable energy supply while, at the same time, stimulating socio-economic development in rural areas [16,17].

Re-cultivating abandoned cropland by bioenergy crops like perennial grasses may reduce atmospheric carbon concentrations from enhanced soil carbon sequestration and fossil fuel substitution [18,19]. In addition to climate mitigation, the conversion of former croplands to perennial grasses can also provide a range of ecological and environmental benefits such as enhanced biodiversity and ecosystem services [16,20], reduced losses of nutrients and soils [21], and local cooling effect due to increased evapotranspiration rates during the growing season [22,23]. At the same time, ground-mounted PV is well suited for deployment on abandoned cropland [24,25]. Utility-scale PV is predicted to play a key role in the sustainable transformation of the global energy systems, and the main reason is the rapid decline in the cost and the technological advancement [26]. However, it is reported that approximately one-third of the total PV farm surface can be covered with solar panels [27–29], as the rest of the area is required for its infrastructure. Covering the land with solar panels may lead to a decline in bio-productivity [30].

Based on the urgent need to transition towards less carbon-intense energy systems [31], spatially-explicit mapping energy potentials of bioenergy and PV is key to understand the future land and energy developments and ultimately stimulate renewable energy production on these areas. In this paper, we address the spatially explicit production of bioenergy and solar photovoltaic for recently abandoned cropland at a global level considering a set of local climate variables, resource yield, and socio-economic feasibility constraints. Global recently abandoned croplands are identified through time series of remotely-sensed land cover maps provided by the European Space Agency (ESA) Climate Change Initiative Land Cover (CCI-LC) [32]. Global primary energy potentials for bioenergy are derived from grid-specific yields of perennial grasses under modern agricultural management practices and site-specific agro-climatic, soil, and terrain conditions using the Global Agro-Ecological Zones (GAEZ) model [33]. For PV, the Centro Euro-Mediterraneo sui Cambiamenti Climatici Climate Model (CMCC-CM) products [34] provide site-specific meteorological data that are used to estimate the primary energy potential [35]. By integrating the gridded primary energy potentials for these renewable energy production options with a spatially explicit Development Potential Index (DPI) [36], we accounted for a range of socio-economic feasibility constraints to provide a more realistic quantification of renewable energy alternatives and identify the optimal use (bioenergy crop or solar PV) per grid cell. The global primary energy potential from an optimal land management at a global level is determined by combining all contributions from bioenergy and PV on the abandoned cropland areas as determined by the DPI. Numerous studies have assessed the resource and land suitability for bioenergy [13,15,30,37–40] or PV [12,14,30,41–43]. These studies focused on specific regions, characteristics and constraints of the different renewable energy production options and identified their contributions to the energy transition. However, to the best of our knowledge, this is the first study that systematically compares with high-resolution data the primary energy potentials from bioenergy crops and PV on abandoned cropland at a global level, and that considers a comprehensive set of local factors and socio-economic constraints to identify the optimal land management for renewable energy production.

2. Methods

2.1. Identification of recently abandoned cropland

The European Space Agency (ESA) Climate Change Initiative Land Cover (CCI-LC) provides global annual data of land cover classes from 1992 to 2015 at a spatial resolution of 10 arc seconds (300 m at the equator) [32]. By combining multiple remote sensing products with ground-truth observations, the ESA CCI-LC maps describe terrestrial surface characteristics through 37 different land cover classes. Six of these classes are cropland or mosaic cropland. We identified abandoned cropland by tracking grid cells transitioning from cropland in 1992 to any non-cropland (and non-urban) class in 2015. In other words, abandoned cropland includes all grid cells that were registered as cropland in 1992 and not in 2015. The cropland grid cells that transitioned to urban land are excluded and not considered as available for renewable energy production, as this is a non-reversible transition.

2.2. Primary bioenergy potential

The bioenergy crops considered here are three promising perennial grasses: switchgrass (*Panicum virgatum*), miscanthus (*Miscanthus x giganteus*), and reed canary grass (*Phalaris arundinacea*). They were selected because they have proven to thrive well on marginal lands due to their suitability to a variety of soil and climate conditions as well as their relatively high yields, low cost and various environmental co-benefits [44–46]. Switchgrass has a C_4 photosynthetic pathway for carbon fixation and can survive in a variety of environmental conditions [47–49]. Switchgrass is native to North America [45,50], but has been introduced in China [46,51,52], Europe [44,48], and many other regions. It is highly adaptive to soil with less fertile, erosive, or acidic conditions, as it has a well-developed root system [46]. However, the species does not cope well under drought conditions [53,54]. The harvesting of switchgrass typically happens throughout autumn [47]. Miscanthus also has a C_4 photosynthetic pathway [47,48]. Miscanthus originated in South-East Asia, but has been introduced in many other regions because of its suitability for establishment in a wide climatic range [49]. Today, miscanthus is present in Europe [48,55], the UK [56], China [52], Turkey [45], among many other regions. Usually, harvesting of miscanthus occurs in late winter or early spring [57,58]. Reed canary grass has a C_3 photosynthetic pathway. It is especially suitable in temperate climates with cool and humid conditions [57,59]. Reed canary grass is currently mainly established in Europe where the species originated [48]. Even in extreme climatic conditions such as floods and droughts, reed canary grass can survive due to its well-adaptive water regime [60]. Similar to miscanthus, the harvest of reed canary grass occurs in late winter or early spring [57,58].

We applied the parameterized crop yield model Global Agro-Ecological Zones 3.0 (GAEZ) to model local yields of bioenergy crops at five arc minutes resolution [61]. GAEZ was developed by the Food and Agriculture Organization (FAO) of the United Nations in collaboration with the International Institute for Applied Systems Analysis (IIASA). GAEZ models dry mass yields based on a variety of crop-specific parameters related to crop characteristics, local soil quality and terrain, agricultural management practices, and site-specific climatic conditions (e.g., radiation, precipitation, and temperature) [33]. It considers the response in crop productivity to yearly variability in soil moisture, pests, frosts and constraints to soil workability. Furthermore, it models the effects of fertilizer use, pesticides, and agricultural conservation measures. Additionally, GAEZ quantify crop water balances, water deficits, and evapotranspiration using the optimal crop growth calendar at rainfed conditions. Based on this, it also models irrigated crop yields by assuming no water deficits throughout the crop growth cycle (i.e. water losses by evapotranspiration do not exceed water absorption at any point). We quantify bioenergy yields for a modern, mechanized and market oriented agricultural management system, with

high yielding varieties, and optimal fertilizer and pesticide use. Maximum attainable dry mass yields for switchgrass, miscanthus, and reed canary grass were computed for both rain-fed and irrigated conditions.

We considered a mixed water supply system with rain-fed water supply in areas threatened by physical water scarcity and irrigation elsewhere. The Aquamaps database [62] provides datasets on physical water scarcity (i.e., when the water demands of the available renewable water resources is not met [63]) at a river basin level. While multiple methods exist to assess water scarcity, the physical water scarcity indicator is especially suitable to address local potentials of new water infrastructure development and measures to increase water use efficiency [64,65]. Additional water withdrawals in areas threatened by water scarcity have higher risks of causing sustainability trade-offs on water depletion. Areas with annual agricultural water use as <10%, 10–20% and >20% of renewable water resources are classified as low, moderate and high physical water scarce, respectively [66]. As an upper irrigation potential, we constrained irrigation deployment to low water scarce areas only.

Applying lower heating values of 17.82 MJ kg^{-1} for switchgrass, 18.55 MJ kg^{-1} for miscanthus, and 18.06 MJ kg^{-1} for reed canary grass [67], we convert dry mass yields to bioenergy yields. By performing an energy-based optimization of the global crop distribution with mixed water supply, each grid is assigned the bioenergy crop with the largest potential. This approach allows to maximize bioenergy yields locally with reduced risks of additional water depletion in water scarce areas.

2.3. Solar photovoltaic primary energy potential

Local PV potentials depend on climatic conditions and nominal installed PV capacity [68]. The incoming solar radiation is the most significant factor for determining the site-specific PV potential [12,69]. Other studies have included additional meteorological conditions such as humidity [70–73], diffuse radiation [74,75], or cloud-cover [76]. The effects of ambient temperature and wind speed are also important for a proper quantification of PV potentials [77,78]. Some previous studies have estimated PV potentials on abandoned cropland at the local and national scale [14,30], but the global PV potential on abandoned cropland is still unclear.

We used the climate data from the Centro Euro-Mediterraneo sui Cambiamenti Climatici Climate Model (CMCC-CM) atmosphere-ocean general circulation model to assess local PV potentials on abandoned cropland [34]. In CMCC-CM, the global circulation is represented by coupling the atmospheric model ECHAM5 [79] and the ocean model OPA8.2 [80], with a resolution of 0.75° and 2°, respectively. Interface between the atmospheric and ocean components is performed by the Ocean Atmosphere Sea Ice Soil version 3 (OASIS3) [81], with a coupling period of 160 min for all parameters. Previous applications of CMCC-CM include assessments of precipitation and cyclones [82], extreme weather [83], vegetation response to climate change [84], and variability of wave power [85]. Spatially explicit climate data on surface downwelling shortwave radiation (RSDS), near-surface air temperature (TAS), and near-surface wind speed (sfcWind) is obtained from the "Atmos" collection of CMCC-CM. Climate model output for the stabilization scenario for Representative Concentration Pathway of 4.5 Wm^{-2} radiative forcing (RCP4.5), with monthly ensemble means from 2010 to 2040 which were aggregated to yearly means served as an estimate for the current climatic conditions. While nominal installed PV capacity is typically provided at standardized conditions (i.e. at a PV cell temperature (T_{cell}) of 25 °C, and RSDS of 1000 Wm^{-2}), the efficiency of PV cells changes with T_{cell} based on local climatic conditions. We apply a parameterized approach to quantify the primary energy potential of a PV deployment on abandoned cropland [35]. The method is widely used and validated through a range of applications [68,86–89].

$$T_{cell}(i,j) = c_1 + c_2 \cdot TAS(i,j) + c_3 + c_4 \cdot sfcWind(i,j) \quad (1)$$

$$PR(i,j) = 1 + \gamma[T_{cell}(i,j) - T_{std}] \quad (2)$$

$$PV_{pot}(i,j) = PR(i,j) \cdot \frac{RSDS(i,j)}{RSDS_{stc}} \quad (3)$$

$$PV_{pri}(i,j) = PV_{pot}(i,j) \cdot P_N \cdot c_{area} \cdot 8760 \quad (4)$$

The site-specific PV potential (PV_{pot}) calculated through Equations (1)–(3) accounts for the ambient effects on T_{cell} of *RSDS*, *TAS*, *sfcWind*, and a set of additional coefficients (Table 1). Further, to obtain the annual primary energy that PV will produce (PV_{pri}) the dimensionless magnitude of PV_{pot} is multiplied with nominal installed power (P_N), the share of solar cells cover of the total land available (c_{area}), and the number of hours in a year (8760) (Equation (4)).

2.4. Development Potential Index for the renewable energy options

Optimal distribution of bioenergy or solar PV on the identified abandoned cropland areas is not only dependent on the primary energy potential, but also on many other factors including biophysical aspects, local land-use or administrative contexts and socio-economic feasibility constraints associated with the intended renewable energy option [9,10,94]. For example, evaluation of local soil characteristics, topography of the landscape and the prevailing climate, as well as grid-specific accessibility to infrastructure, markets, and other socio-economic conditions, are key factors that affect priorities among different renewable energy options [11].

In order to take these aspects into account, Oakleaf et al. [36] introduced the Development Potential Index (DPI), which incorporates site-specific development constraints and criteria when determining the land suitability for development of the given renewable energy option. Spatially explicit DPIs are available for 13 renewable energy sources, including bioenergy and PV. By applying a multi-criteria decision analysis technique integrated with geographic information systems [93], site-specific suitability is mapped globally with a 1 km resolution. DPIs include various development constraints associated with the specific resource, land-use and biophysical criteria, technical yields, feasibility criteria (e.g., major roads, electrical grid, and demand centers), and feasibility measures (e.g., logistics), which differ by location and type of renewable energy option considered. All these factors are integrated in terms of relative importance through an analytic hierarchy process [95] combined with a weighted linear combination method [93], so that the computed normalized spatial DPI values range between 0 and 1. For PV, energy yields and distance to electrical grids contribute the most to DPI values (weighted 0.447 and 0.228, respectively). Landcover characteristics (0.115), distance to urban areas (0.069), and distance to railways and ports (0.026) are also included in the parameterization. Bioenergy DPIs are quantified based on bioenergy crop yields (0.493), market accessibility (0.311) and land supply elasticity (0.196) [36].

We overlapped the DPIs for bioenergy and PV based on Oakleaf et al. [36] with our identified maps of abandoned cropland to quantify their development potentials. We used ESRI ArcGIS Desktop 10.8 [96] to remap DPI data from the Mollweide coordinates system to the WGS 1984 coordinate system. It was possible to directly assign DPI values for bioenergy and PV to

Table 1
Parameters for estimating spatially explicit PV primary energy potential.

Notation	Value	Unit	Description	Reference
c_1	4.3	$^{\circ}C$	Response coefficient accounting for climate effects	[68,90]
c_2	0.943	-	Response coefficient accounting for climate effects	[68,90]
c_3	0.028	$^{\circ}Cm^2W^{-1}$	Response coefficient accounting for climate effects	[68,90]
c_4	−1.528	$^{\circ}Csm^{-1}$	Response coefficient accounting for climate effects	[68,90]
γ	−0.005	$^{\circ}C^{-1}$	Maximum power thermal coefficient	[35,68,91]
T_{std}	25	$^{\circ}C$	Standard test conditions of PV cell temperature	[68,90]
$RSDS_{stc}$	1000	Wm^{-2}	Standard test conditions of *RSDS*	[68,90]
P_N	110	W_pm^{-2}	Nominal power (or Watt peak)	[27,28,92,93]
c_{area}	0.33	-	PV coverage of total land available	[27–29]

47 Mha and 56 Mha of abandoned cropland, respectively, and there were 40 Mha of abandoned cropland for which it was possible to assign DPI values for both renewable energy sources. For some areas of abandoned cropland, it was thus not possible to assign a given DPI value owing to missing entries in the original DPI dataset, e.g., for latitudes 60–90 °N. We applied a data filling method to quantify DPI values of these abandoned cropland areas by taking the moving mean of surrounding grid cells for a range of different window sizes (from 3 × 3 to 31 × 31 cell windows). With a window size of 3 × 3 cells that only considers the nearest neighbor cells, the extent of abandoned cropland with DPI values for bioenergy and PV increases from 40 Mha to 67 Mha. Across all assessed window sizes, we obtain DPI values for both bioenergy and PV for an additional 27–40 Mha of abandoned cropland. This increases total DPI coverage up to 67–80 Mha. Supplementary Fig. 1 shows that while there are rapid gains in abandoned cropland with DPI values at smaller window sizes, the curve quickly starts to converge towards 80 Mha. The remaining 3 Mha of abandoned cropland are located within larger clusters of missing values such as seen in parts of northern Africa and eastern Asia. We have thus identified the 11 × 11 cell window (about 1 ° × 1 °) as the best option to balance trade-offs between lower areas with DPI coverage and increased uncertainties related to data filling by taking DPI values from far areas within larger clusters. This choice results in 78 Mha (out of the 83 Mha identified globally) of abandoned cropland with assigned DPI values for both bioenergy and PV.

By comparing the spatially explicit DPIs for bioenergy and PV on abandoned cropland, the optimal combination for renewable energy production on abandoned cropland is determined. The energy potentials described in section 2.2 and 2.3 are applied to each given grid cell so that the bioenergy potential is computed for areas where the bioenergy DPI is higher than the DPI for PV, and the PV potential for areas where DPI for PV is higher than bioenergy DPI. Further, a sensitivity analysis explores the land requirements and energy potentials across different DPI thresholds (i.e., deploying energy production on all areas with DPI values above a given threshold), and the effect of the data filling method on the global potentials. The DPI-optimized land allocation to bioenergy and PV, the corresponding mean energy yields, and total energy potentials on abandoned cropland is therefore computed for a range of window sizes between 3 × 3 and 31 × 31 cells.

3. Results and discussion

3.1. Abandoned cropland

A total of 83 Mha of abandoned cropland globally can be identified from the ESA CCI-LC land cover maps between 1992 and 2015 (Fig. 1). Most of these areas are located in Asia (30%), followed by Americas (28%), Africa (22%), Europe (20%), and, lastly, Oceania (5%). Drivers behind abandonment of agricultural land are many and include environmental, socio-economic and political factors [97,98]. Natural geophysical constraints, such as a decline in soil quality and land degradation, may motivate the cropland abandonment [15,98] as well as topography (e.g., mountain regions and dry areas) [99]. Nevertheless, socio-economic drivers are of larger importance. Lack of availability of critical infrastructure (such as roads) and missing subsidies for farming may force landowners to give up the land [98]. Abandonment of cropland may also result from changes in internal or external politics (e.g., migration of land-use activities to less developed countries [100]), and the shift towards market-driven economies (e.g., the dissolution of the Soviet Union) [99].

In Asia, we find intensive cropland abandonment in Southeast regions close to the equator (e.g., Malaysia and Indonesia). Smaller fractions of abandoned cropland are found in North and Central America, and along the coast of South America. In Africa, regions just south of the equator, such as Congo, Angola, and Tanzania, have large areas of abandoned cropland. In Europe, large areas of abandoned cropland are found in the former Soviet Union (e.g., Russia, Ukraine, and Kazakhstan) and eastern parts of Europe. Also, abandonment of farming occurs in Oceania, mainly along the coastlines of Australia and New Zealand.

3.2. Primary energy potential of bioenergy and PV

Annually, global bioenergy potentials on abandoned cropland are estimated to be 35 EJ (Fig. 2a), assuming modern agricultural practices and irrigation in areas with no physical water scarcity. This means that in water scarcity areas where the abandoned cropland is not suitable to rain-fed bioenergy crops (about 5 Mha), there is no bioenergy potential. On the other hand, PV farms on

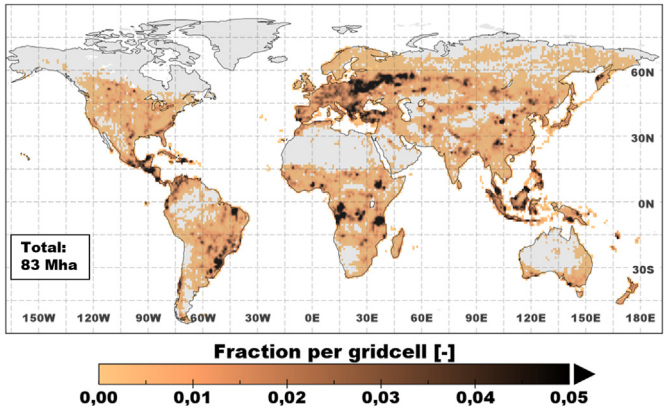

Fig. 1. Globally identified abandoned cropland between 1992 and 2015. The color bar shows the grid cell fraction at 1° resolution (aggregated from the resolution of the original dataset for visualization purposes). (For interpretation of the references to color in this figure legend, the reader is referred to the Web version of this article.)

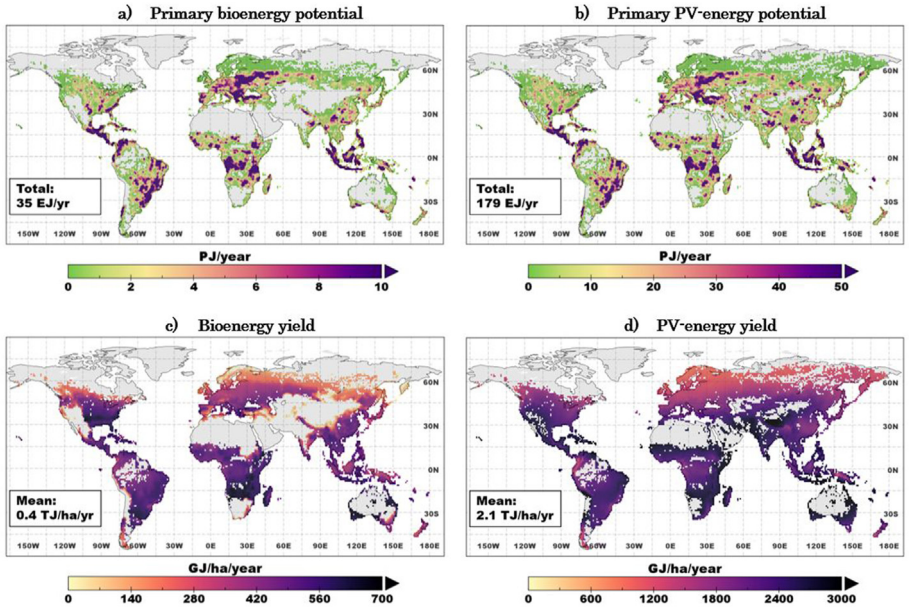

Fig. 2. Primary energy potentials on abandoned cropland for bioenergy (a) and PV-energy (b), in PJ year^{-1} and energy yield (i.e., energy output per hectare of land) for bioenergy (c) and PV-energy (d) in GJ ha^{-1} year^{-1}. Note that scales of the color bars are different for each panel. (For interpretation of the references to color in this figure legend, the reader is referred to the Web version of this article.)

abandoned cropland can produce 179 EJ year^{-1} (Fig. 2b), which is more than five times higher than the bioenergy potential. The mean primary energy yield of bioenergy is 0.4 TJ ha^{-1} year^{-1} (Fig. 2c) and for PV 2.1 TJ ha^{-1} year^{-1} (Fig. 2d).

For all locations of abandoned cropland, the potential primary energy output is higher for PV compared to bioenergy; however, the magnitude by which PV performs better than bioenergy differs regionally. A clear latitudinal trend can be identified: bioenergy performs better in the tropics (where yields are high) compared to higher latitudes, even though it does not out-compete PV. The highest bioenergy yields are located in the west coast of South America, Africa, and Southeast Asia. However, a significant bioenergy potential is also found in eastern parts of Europe and some locations in Central America. Areas with high PV potential are widely scattered. The main productive regions include the east coast of South America, Central America, parts of Africa, mid-Europe and South East Asia. The lowest PV yields are found in Scandinavia and North America.

3.3. Development Potential Index for bioenergy and PV

We mapped Development Indices (DPIs), a measure of technical and socioeconomic feasibility, of bioenergy and PV from Oakleaf et al. [36] on the identified areas of abandoned cropland (Fig. 3). Average DPI for bioenergy across abandoned cropland is found to be 0.53 (Fig. 3a), while it is 0.58 for solar PV (Fig. 3b). This result indicates that globally the development of solar PV farms on abandoned cropland has a slightly higher development potential compared to bioenergy. However, bioenergy is more suitable compared to PV in some areas due to several local biophysical and socio-economic feasibility factors considered in the DPI. In general, the highest DPI for bioenergy on abandoned cropland are located in tropical and mild temperate regions, while the development potential for PV is higher in dryer climatic conditions. By investigating the differences between DPI for PV and DPI for bioenergy on abandoned cropland per grid cell (Fig. 3c) we find a mean global difference of 0.05. The difference in DPI per grid cell is closer to zero around the equator (mainly in Africa and South America) and in Central-Europe, among other regions (light blue and yellow color in Fig. 3c). The DPI of PV is higher than the DPI of bioenergy in large parts of sub-Saharan Africa, North America, the eastern Part of South America, Central Asia and the eastern parts of Australia (red color in Fig. 3c). In contrast, the DPI of bioenergy is higher than the DPI of PV for areas such as the western and middle parts of South America, South-East Asia, and some clusters in Europe, Africa and Australia (dark blue color in Fig. 3c).

3.4. Optimal deployment of bioenergy and PV based on DPIs

By comparing the site-specific DPIs, an optimal distribution of bioenergy and PV deployment for renewable energy production is determined (Fig. 4) for 78 Mha of the initial 83 Mha abandoned cropland. The remaining 5 Mha has no DPI due to the selected size of the window for the data filling methods. The influence of alternative window sizes is explored in a sensitivity analysis. The results show that 68% (53 Mha) of the abandoned cropland have higher suitability for establishment of PV infrastructure, while the other 32% (25 Mha) is more suitable for bioenergy deployment (Fig. 4a). An optimal DPI-based deployment of these two renewable energy options has a primary energy potential of 125 EJ year^{-1} at a global level, of which 114 EJ year^{-1} are from PV and 11 EJ year^{-1} from bioenergy. Therefore, a significantly higher share of the total energy generated will come from PV deployment (91%) compared to bioenergy (9%). We find that the optimal land management of abandoned cropland combining PV and bioenergy will have DPI values greater than 0.1 for all locations (Fig. 4b and c). However, most of the primary energy potential is associated with land areas with a DPI ranging from 0.4 to 0.8, and only a tiny fraction of the land will have a DPI close to 1 (i.e., maximum development potential).

While the overall optimal deployment for PV and bioenergy is quite fragmented (Fig. 4a), some trends can be observed. North America and a large part of Central and South America have a higher development potential for PV compared to bioenergy. In Europe, the Mediterranean countries are more suitable for PV than bioenergy deployment. In contrast, bioenergy has larger DPI values in Great Britain, Ireland, Poland, and the former Soviet states except

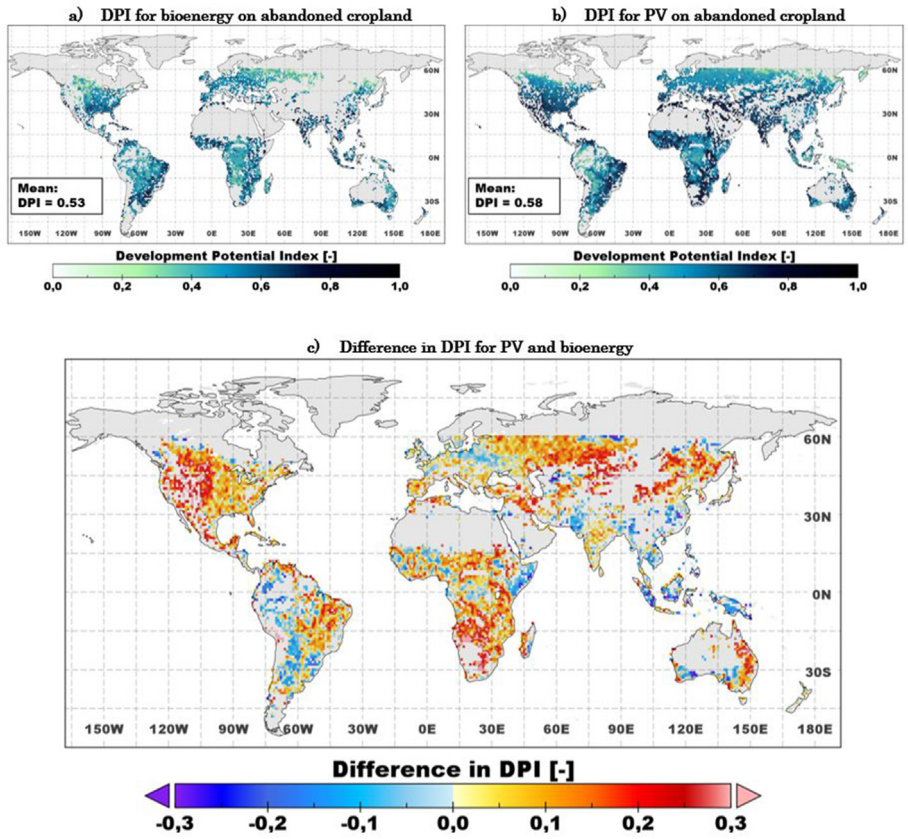

Fig. 3. Development Potential Index (DPI) on abandoned cropland for bioenergy (a), PV-energy (b) and (c) difference between DPI for PV and DPI for bioenergy on (cells of) abandoned cropland. Range for DPI is between 0 and 1, where 1 represent maximum development potential. DPIs are based on Oakleaf et al. [36] and applied to the identified abandoned cropland areas. The difference in DPI is calculated as DPI of PV minus the DPI of bioenergy per grid cell. This means that if a grid cell has a value greater than zero it has a higher DPI for PV than for bioenergy.

for Russia. In the African continent, bioenergy is a better option in the eastern part of the Horn of Africa, western and central Africa, while PV is the preferred option under the equator. Large parts of Asia have a higher development potential for PV, but some exceptions are in Pakistan, China, and Southeastern Asia. Further, we find that the eastern states of Australia and New Zealand have a higher potential for PV. Along a latitudinal gradient, the areas between 30 and 60°N have a higher PV potential while most of the tropical areas situated around the equator have a higher bioenergy potential. In total, 125 EJ year^{-1} of primary energy can be generated, at a global mean primary energy potential of 1.6 TJ ha^{-1} year^{-1} for an optimal deployment of abandoned cropland areas (Fig. 4d and e). This potential is produced with an average DPI of 0.61 (Fig. 4f). This value is higher than the mean DPI when only deployment of bioenergy (mean DPI 0.53) or PV (mean DPI 0.58) is considered (see Fig. 3a and b), meaning that an optimal allocation of renewable energy production to abandoned cropland on the basis of the DPI offers higher potentials of development.

This primary energy potential from abandoned cropland can be compared to the expected renewable energy deployment in future climate change mitigation scenarios. The projected median renewable primary energy needed to limit global warming to 1.5 °C across different SSPs in 2100 is 224–412 EJ year^{-1} from biomass and 54–243 EJ year^{-1} from solar energy [5,6]. Comparing these estimates to our result of bioenergy (11 EJ year^{-1} under DPI-based optimal land allocation), it is clear that limiting bioenergy production to abandoned cropland is not sufficient. More resources from forest residues, waste products, or bioenergy crops produced on current cropland or pastureland are needed to reach the projections across all SSPs. However, deployment of perennial grasses on abandoned cropland is a promising near-term option that can facilitate a gradual upscale of bioenergy production from second generation feedstocks. On the other hand, our estimate of 114 EJ year^{-1} for PV represents a large share of the expected PV demand, and in one scenario (SSP4) it can cover all the projected solar energy demand. It also covers large parts of the 2100 demand in SSP1 and SSP2 (83% and 78%, respectively), and 47% of the demand in the energy intensive SSP5 scenario where a delayed energy transition leads to an extensive deployment of renewable energy sources in the second half of the century [6].

3.5. Development Potential Index thresholds and land-energy interactions

There are non-linear relationships between DPI-thresholds, land availability and energy potentials (Fig. 5). Half of the abandoned cropland is located in areas where DPI is higher than 0.53 and 0.60 for bioenergy (Fig. 5a) and PV (Fig. 5b), respectively. With DPI optimized land management, there is relatively higher land availability for energy production at a given DPI threshold (Fig. 5c). Half of the abandoned cropland can be utilized at a DPI threshold of 0.63, with 13 Mha and 26 Mha allocated to bioenergy and PV, respectively. Abandoned cropland with DPI above 0.8 is limited for both bioenergy and PV (2.4 Mha and 1.7 Mha, respectively). Even in the DPI optimized scenario, only 3.8 Mha of the abandoned cropland has DPI above 0.8 (2.3 Mha and 1.5 Mha allocated to bioenergy and PV, respectively). At the same time, 85%, and 95% of abandoned cropland has DPI above 0.4 for bioenergy and PV, respectively. The

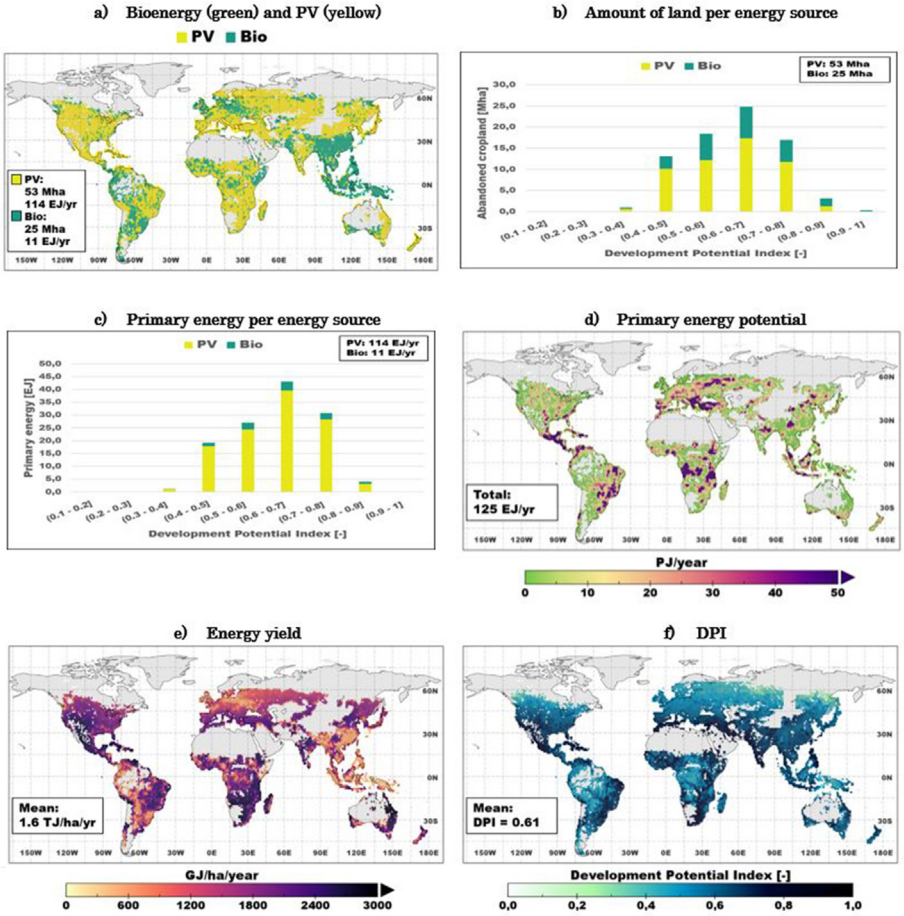

Fig. 4. Optimal allocation to abandoned cropland of PV and bioenergy based on the Development Potential Index (DPI). Areas identified with higher DPI for PV in yellow and bioenergy in green (a). Amount of hectares of land (b) and primary energy production (c) for the optimal management of PV (yellow) and bioenergy (green) by ranges of DPIs. Primary energy potential per year (in PJ year^{-1}) (d) and energy yield (in GJ ha^{-1} year^{-1}) (e) for optimal management of abandoned cropland. (f) Development Potential Index (DPI) for optimal land management on abandoned cropland for renewable energy production by bioenergy and PV. (For interpretation of the references to color in this figure legend, the reader is referred to the Web version of this article.)

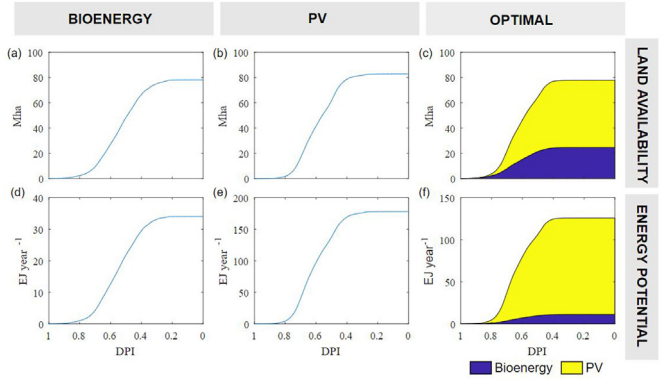

Fig. 5. Relationship between DPI levels, land availability and achievable primary energy potentials assuming all abandoned cropland above a given DPI is utilized for energy production. Land availability [Mha] are shown for (a) bioenergy, (b) PV, and (c) for the DPI optimized allocation of bioenergy and PV on abandoned cropland. Maximum land availability differs slightly between scenarios due to variations in DPI data availability. Energy potentials [EJ year^{-1}] are shown for (d) bioenergy, (e) PV, and (f) the DPI optimized allocation of bioenergy and PV on abandoned cropland. Note different scales on y-axis for energy potentials in (d), (e) and (f).

optimized land management make use of 99% of abandoned cropland above a 0.4 DPI threshold, with 24 Mha and 53 Mha allocated to bioenergy and PV, respectively.

Reaching half of the bioenergy potential requires a DPI threshold of 0.55 and 37 Mha of abandoned cropland, with a mean bioenergy yield of 460 GJ ha^{-1} year^{-1} (Fig. 5d). Half the PV potential is achievable with a DPI threshold of 0.61 by utilizing 39 Mha of abandoned cropland, and a mean PV energy yield of 2349 GJ ha^{-1} year^{-1} (Fig. 5e). With optimal land management, half of the energy potential is reached at a higher DPI threshold of 0.64 (Fig. 5f). This requires 12 Mha and 25 Mha to produce 5.8 EJ year^{-1} and 59.5 EJ year^{-1} for bioenergy and PV, respectively. Mean energy yields increase slightly at a 0.64 DPI threshold to 467 GJ ha^{-1} year^{-1} and 2380 GJ ha^{-1} for PV and bioenergy, respectively.

The top 10 percentiles of the energy potentials are achievable at DPI thresholds of 0.71, 0.74 and 0.76, with land requirements of 8.1 Mha, 7.5 Mha and 9.5 Mha to produce 3.6 EJ year^{-1}, 19 EJ year^{-1} and 13 EJ year^{-1} for bioenergy, PV and optimal land management, respectively. In the optimal land management scenario, 1.7 EJ year^{-1} and 11 EJ year^{-1} is produced with mean energy yields of 439 GJ ha^{-1} year^{-1} and 2481 GJ ha^{-1} year^{-1} for bioenergy and PV, respectively. On the other hand, 90% of the total potential is reachable with DPI threshold of 0.38, 0.44 and 0.47, thereby producing 30 EJ year, 161 EJ year^{-1} and 114 EJ year^{-1} with land requirements of 69 Mha, 74 Mha and 70 Mha for bioenergy, PV and optimal land management, respectively. With optimal land management, 10 EJ year^{-1} and 103 EJ year^{-1} is produced, with mean energy yields of 454 GJ ha^{-1} year^{-1} and 2196 GJ ha^{-1} year^{-1} for

bioenergy and PV, respectively.

While PV energy yields peak at a 0.96 DPI threshold for the optimal land management scenario (2825 GJ ha^{-1} year^{-1}), we find that mean bioenergy yields peak at a DPI threshold of 0.63 (466 GJ ha^{-1} year^{-1}). This indicates that market accessibility or land supply elasticity (i.e. the relationship between land use change, and land and crop prices) might be a constraint in some of the highest yielding areas for bioenergy production. Furthermore, we deploy irrigated bioenergy production in areas that are not threatened by water scarcity, which is not directly reflected by the DPI values.

3.6. Uncertainty and limitations

We performed a sensitivity analyses to assess the effects of the DPI data filling method on areas of abandoned cropland with an assigned DPI value and the resulting primary energy potentials. Supplementary Table 1 shows how results vary according to different sizes of the moving window (between 3 × 3 to 31 × 31 cell windows). Across all the window sizes considered, we obtained DPI values for an additional 27–40 Mha. Including these additional cells brings total abandoned cropland with both bioenergy and PV DPIs to 67–80 Mha, with optimal energy potentials ranging between 107 and 129 EJ year^{-1}. While a larger window size increases both the considered land availability and energy potentials, it does not affect the share of land distributed between bioenergy and PV. Allocated shares of abandoned cropland to bioenergy and PV are 31–32% and 68–69% across all considered window sizes, respectively. This indicates an even spread of missing values across the abandoned cropland grids. Likewise, mean bioenergy and PV energy yields show small variations (454–457 GJ ha^{-1} and 2130–2153 GJ ha^{-1}, respectively). Contributions to optimal total energy production stay at 9% and 91% for bioenergy and PV, respectively.

The recently released ESA CCI-LC products aim to give a more realistic representation of land cover dynamics compared to former datasets by resolving some of their limitations [101,102]. Several previous studies validated the accuracy of the ESA CCI-LC dataset. The global overall accuracy is 71% [103], but with some regional differences. Overall accuracies are 72% in China [104], 62% in Africa [105], 70% in South America [105], 62% in the Arctic [106] and 84% in coastal Eurasia [107]. Cropland classes have the highest global accuracy. Median global user and producer accuracies of cropland classes are 89% and 80%, respectively [103]. The ESA CCI-LC dataset is also found to be broadly consistent with other cropland identification approaches [105,108]. This makes the ESA CCI-LC especially useful for cropland monitoring, with both a relatively high precision in total cropland extent, and a high spatial cropland match. Moreover, the estimates of a detected change in terrestrial surface are based on changes registered over a two year period, so that temporary changes (e.g., a short period of extreme events such as draughts) will not affect the data, and this is considered a strength of the CCI-LC database. An increasing number of studies rely on the ESA CCI-LC products for analysis of effects of land cover changes. Examples include effects of recent land-use and land-cover changes on the terrestrial carbon stocks [102,109], air temperature and humidity effects [110], surface energy budget [109], assessments of global cropland sparing potentials [111], global urban expansion [112], and land cover changes within biodiversity hotspots [113].

The GAEZ model relies on complex databases to provide spatial agro-climatic yields, and both the databases and the assumptions in the model itself have intrinsic uncertainties [33]. Despite this, the GAEZ model is widely tested, validated and used in multiple applications [114–118]. In order to estimate the bioenergy potential on abandoned cropland, the energy-based optimal solution for perennial grasses allocation in combination with high agricultural management levels and mixed water supply system is utilized. Bioenergy potentials are lower if a low or medium agriculture management intensity is considered (e.g., lower inputs of nutrients, lower mechanization of field work, etc.), but higher if irrigation is deployed on all abandoned cropland. More refined estimates of bioenergy potentials can be achieved with regional analysis that considers local trade-offs with economic and environmental factors to identify the best management practice.

Meteorological data from CMCC-CM rely on the atmospheric model ECHAM5 [79] and the ocean model OPA8.2 [80] coupled by the OASIS3 interface [81]. As each of the models are combined to create the CMCC-CM, the datasets from CMCC-CM include the intrinsic uncertainties related to each model and those from their combination [82]. The primary energy potential for PV is estimated based on two main assumptions that are subject to uncertainties: the nominal installed power [27,28,92,119] and the amount of area covered by solar panels [27–29]. These parameters can be adjusted to represent advancements in technologies or by accounting for site-specific conditions. The primary energy potential of PV also depends on solar radiation, ambient temperature, cell temperature, and wind speed, and future changes in background climatic conditions can influence productivity of PV. Nominal installed production, area covered with solar cells and technical parameters like orientation, tilt, and incline of the PV modules also affect estimates of potentials [120]. Typically, PV systems using a tracking system that follow the sun path compared to fixed orientation can gain higher efficiency [121].

Regarding the DPI data, the uncertainty of model outputs as well as the sensitivity to model inputs have been investigated in the original study that produced the DPI dataset [36]. The study also validated the DPIs by investigating recent or planned developments by using more than 6000 data-points and 200,000 km^2 of mapped locations. A Monte Carlo approach determined the uncertainty, and the mean coefficient of variation for bioenergy DPI (0.137) is higher compared to the mean coefficient of variation for PV DPI (0.048). In general, lower uncertainty is found for higher DPI areas. For PV, high uncertainty is typically associated with areas in remote regions that lacked supporting infrastructure or market access but had higher than average resource potential (i.e., yield criteria in all DPIs). For bioenergy, the highest uncertainty values mainly occurred in regions with lower yields and longer distances to markets or infrastructure.

Additional work can explore the optimal DPI land management on abandoned cropland under the changing climate niche [122]. As energy yield is the most important parameter in the DPI methodology for PV and bioenergy [36], and are depending on climate conditions, future climate changes will likely affect the optimal land allocation and energy potentials. Bioenergy dry mass yields are projected to decrease globally in the 21st century for rain-fed bioenergy crops in RCP4.5 and RCP8.5, with the magnitude of change being almost double in RCP8.5 relative to RCP4.5 [123]. The largest declines are projected in the tropics and subtropics, but there are also increasing yields projected at higher latitudes in parts of the northern hemisphere. Global crop yield losses can to some extents be mitigated through irrigation deployment and genetic modifications [123–125]. For PVs, cell efficiency decreases with increased cell temperatures and cloud cover but increase with increased incoming solar radiation [126]. Global PV energy yields are expected to decrease globally as a response to climate change [69]. For example, mean PV potentials are projected to decrease towards 2100 in RCP8.5 with −10% and −4% in Europe [68] and Africa [89], respectively.

Although our analysis only focused on renewable energy potentials, there are multiple local environmental effects associated with bioenergy or solar PV deployment that are important to

consider, and that can differ significantly between the two options. There are several environmental benefits that can be obtained by introducing dedicated bioenergy crops on former cropland. For example, lower nutrient and soil losses [50], and supporting several ecosystem services [44]. On the other hand, producing solar energy with photovoltaic panels on open land is sometimes heavily contested because of nature protection, accessibility, and cultural heritage [42].

Deployment strategies for renewable energy options are highly influenced by political and economic factors [16]. Local, national or international laws, regulations, and subsidies can either promote or inhibit renewable energy deployment. The integration of ESA CCI-LC and DPIs allows assessing opportunity costs and the potential of a land-use conversion from abandoned cropland to energy production. The results of our spatially explicit analysis offer the opportunity to zoom into different local and regional contexts. As the DPI methodology is especially suitable to identify priority regions for new deployment of renewable energy infrastructure [36], our findings show the potential hidden at low risks for rising competition for land and provide a preliminary screening of the key regions with extensive cropland abandonment that can be prioritized for bioenergy or PV deployment. Implementation of these solutions should consider the specific local factors for sustainable land management and energy planning at the local level, and involve environmental and socio-economic indicators other than those included in the analysis (e.g., resource availability, material requirements, biodiversity, social factors, political factors, energy system characteristics or property rights). For example, bioenergy crops are found to improve many indicators of ecosystem services relative to cropland (including biodiversity), whereas PV panels would have a likely more detrimental effects on terrestrial ecosystems on which they are established. Further, the inclusion of other renewable energy sources in the analysis may change the optimal allocation of renewable energy options to specific grid cells, and likely lead to overall increased DPI values on abandoned cropland. For example, abandoned cropland may be more suitable for wind energy production [14], or could contribute to the deployment of new hydropower reservoirs [127].

4. Concluding remarks

This study provided a detailed analysis of the optimal land management on abandoned cropland for renewable energy production considering bioenergy or solar PV deployment. By only considering the potential primary energy output of each renewable energy option, the PV potential far outcompetes the one of bioenergy crops at a global level. However, the consideration of different biophysical and socio-economic factors provides a more realistic comparison and deployment potential. Considering site-specific DPIs, a mix of bioenergy and PV is found to be the best solution for renewable energy production on abandoned cropland. About 68% of the total area of abandoned cropland favors the deployment of solar PV farms, and the rest (32%) favors the establishment of bioenergy. In total, the optimal land management on abandoned cropland can potentially produce 125 EJ primary energy per year, where 91% (114 EJ year^{-1}) is from PV and 9% (11 EJ year $^{-1}$) from bioenergy. Further, an optimal allocation of renewable energy production to abandoned cropland on the basis of the DPI offers higher potentials of development than considering the deployment of an individual option (either PV or bioenergy). Overall, the estimated bioenergy potentials under this optimal management of abandoned cropland are not sufficient to meet a large share of the expected bioenergy demand from long-term projections in 1.5 °C future scenarios. On the other hand, the estimates of PV potentials cover almost all the 2100 PV demand in SSP1-1.9 and makes a substantial contribution even in the energy intensive SSP5-1.9 scenario (47%).

To meet the Paris Agreement's goals and, at the same time, provide a significant energy supply for a sustainable future, renewable energy production from large-scale deployment of both bioenergy from perennial grasses and PV technologies is a critical factor. Bioenergy and PV have non-negligible potentials for primary energy production on abandoned cropland, which can be used to guide an early phase deployment of large-scale renewable energy production at lower risks of competition with environmental protection and food security. We show that there is an optimal mix for the implementation of these two options at a global level under a range of biophysical and socio-economic indicators. Targeted measures can stimulate the production of renewable energy, taking into consideration the local context for implementing the most suitable options in each specific region. Site-specific analyses considering sustainability indicators, regional conditions, and the international political arena are instrumental for determining tailor-made implementation practices for renewable energy productions. Future research integrating aspects of land use sciences, energy sciences, and social sciences connected to different renewable energy options and local contexts are necessary for promoting more assertive sustainable land management strategies for the energy transition required to meet the most ambitious targets for renewable energy production and GHG emission reduction.

CRediT authorship contribution statement

Malene Eldegard Leirpoll: Writing - original draft, Writing - review & editing. **Jan Sandstad Næss:** Writing - review & editing. **Otavio Cavalett:** Validation, Writing - review & editing. **Martin Dorber:** Resources. **Xiangping Hu:** Resources. **Francesco Cherubini:** Supervision, Funding acquisition, Writing - review & editing.

Declaration of competing interest

The authors declare that they have no known competing financial interests or personal relationships that could have appeared to influence the work reported in this paper.

Acknowledgments

We acknowledge the support of the Norwegian Research Council through the projects BioPath (no. 294534), Bio4Fuels (no. 257622), and MitiStress (no. 286773). We gratefully acknowledge the provision of spatial land-cover data by the ESA-CCI Land Cover project, bioenergy yield data from GAEZ, climate data from CMCC-CM, and DPI data from Oakleaf et al.

Appendix A. Supplementary data

Supplementary data to this article can be found online at https://doi.org/10.1016/j.renene.2020.11.159.

References

[1] V. Masson-Delmotte, P. Zhai, H.O. Pörtner, D. Roberts, J. Skea, P.R. Shukla, A. Pirani, W. Moufouma-Okia, C. Péan, R. Pidcock, S. Connors, J.B. Matthews, Y. Chen, X. Zhou, M.I. Gomis, E. Lonnoy, T. Maycock, M. Tignor, T. Waterfield, Summary for policymakers, in: Global Warming of 1.5°C. An IPCC Special Report on the Impacts of Global Warming of 1.5°C above Pre-industrial Levels and Related Global Greenhouse Gas Emission Pathways, in the Context of Strengthening the Global Response to, 2018. https://report.ipcc.ch/sr15/pdf/sr15_spm_final.pdf%0Ahttp://www.ipcc.ch/report/sr15/.

[2] IEA 2020, Global Energy Review 2019, Iea, 2019. https://www.iea.org/reports/global-energy-review-2019.

[3] IRENA, Global energy transformation: a roadmap to 2050. http://irena.org/publications/2018/Apr/Global-Energy-Transition-A-Roadmap-to-2050%0Awww.irena.org, 2019.
[4] A. Popp, K. Calvin, S. Fujimori, P. Havlik, F. Humpenöder, E. Stehfest, B.L. Bodirsky, J.P. Dietrich, J.C. Doelmann, M. Gusti, T. Hasegawa, P. Kyle, M. Obersteiner, A. Tabeau, K. Takahashi, H. Valin, S. Waldhoff, I. Weindl, M. Wise, E. Kriegler, H. Lotze-Campen, O. Fricko, K. Riahi, D.P. va Vuuren, Land-use futures in the shared socio-economic pathways, Global Environ. Change 42 (2017) 331–345, https://doi.org/10.1016/j.gloenvcha.2016.10.002.
[5] K. Riahi, D.P. van Vuuren, E. Kriegler, J. Edmonds, B.C. O'Neill, S. Fujimori, N. Bauer, K. Calvin, R. Dellink, O. Fricko, W. Lutz, A. Popp, J.C. Cuaresma, S. KC, M. Leimbach, L. Jiang, T. Kram, S. Rao, J. Emmerling, K. Ebi, T. Hasegawa, P. Havlik, F. Humpenöder, L.A. Da Silva, S. Smith, E. Stehfest, V. Bosetti, J. Eom, D. Gernaat, T. Masui, J. Rogelj, J. Strefler, L. Drouet, V. Krey, G. Luderer, M. Harmsen, K. Takahashi, L. Baumstark, J.C. Doelman, M. Kainuma, Z. Klimont, G. Marangoni, H. Lotze-Campen, M. Obersteiner, A. Tabeau, M. Tavoni, B.C. O'Neill, S. Fujimori, N. Bauer, K. Calvin, R. Dellink, O. Fricko, W. Lutz, A. Popp, J.C. Cuaresma, S. KC, M. Leimbach, L. Jiang, T. Kram, S. Rao, J. Emmerling, K. Ebi, T. Hasegawa, P. Havlik, F. Humpenöder, L.A. Da Silva, S. Smith, E. Stehfest, V. Bosetti, J. Eom, D. Gernaat, T. Masui, J. Rogelj, J. Strefler, L. Drouet, V. Krey, G. Luderer, M. Harmsen, K. Takahashi, L. Baumstark, J.C. Doelman, M. Kainuma, Z. Klimont, G. Marangoni, H. Lotze-Campen, M. Obersteiner, A. Tabeau, M. Tavoni, The Shared Socioeconomic Pathways and their energy, land use, and greenhouse gas emissions implications: an overview, Global Environ. Change 42 (2017) 153–168, https://doi.org/10.1016/j.gloenvcha.2016.05.009.
[6] J. Rogelj, A. Popp, K.V. Calvin, G. Luderer, J. Emmerling, D. Gernaat, S. Fujimori, J. Strefler, T. Hasegawa, G. Marangoni, V. Krey, E. Kriegler, K. Riahi, D.P. Van Vuuren, J. Doelman, L. Drouet, J. Edmonds, O. Fricko, M. Harmsen, P. Havlík, F. Humpenöder, E. Stehfest, M. Tavoni, Scenarios towards limiting global mean temperature increase below 1.5 °c, Nat. Clim. Change 8 (2018) 325–332, https://doi.org/10.1038/s41558-018-0091-3.
[7] P. Smith, K. Calvin, J. Nkem, D. Campbell, F. Cherubini, G. Grassi, V. Korotkov, A. Le Hoang, S. Lwasa, P. McElwee, E. Nkonya, N. Saigusa, J.F. Soussana, M.A. Taboada, F.C. Manning, D. Nampanzira, C. Arias-Navarro, M. Vizzarri, J. House, S. Roe, A. Cowie, M. Rounsevell, A. Arneth, Which practices co-deliver food security, climate change mitigation and adaptation, and combat land degradation and desertification? Global Change Biol. 26 (2020) 1532–1575, https://doi.org/10.1111/gcb.14878.
[8] L.R. Boysen, W. Lucht, D. Gerten, Trade-offs for food production, nature conservation and climate limit the terrestrial carbon dioxide removal potential, Global Change Biol. 23 (2017) 4303–4317, https://doi.org/10.1111/gcb.13745.
[9] R. Thomas, M. Reed, K. Clifton, N. Appadurai, A. Mills, C. Zucca, E. Kodsi, J. Sircely, F. Haddad, C. Hagen, E. Mapedza, K. Woldearegay, K. Shalander, M. Bellon, Q. Le, S. Mabikke, S. Alexander, S. Leu, S. Schlingloff, T. Lala-Pritchard, V. Mares, R. Quiroz, A framework for scaling sustainable land management options, Land Degrad. Dev. 29 (2018) 3272–3284, https://doi.org/10.1002/ldr.3080.
[10] F. Poggi, A. Firmino, M. Amado, Planning renewable energy in rural areas: impacts on occupation and land use, Energy 155 (2018) 630–640, https://doi.org/10.1016/j.energy.2018.05.009.
[11] J. Malczewski, GIS-based land-use suitability analysis: a critical overview, Prog. Plann. 62 (2004) 3–65, https://doi.org/10.1016/j.progress.2003.09.002.
[12] Y. Choi, J. Suh, S.-M. Kim, GIS-based solar radiation mapping, site evaluation, and potential assessment: a review, Appl. Sci. 9 (2019), https://doi.org/10.3390/app9091960.
[13] C.B. Field, J.E. Campbell, D.B. Lobell, Biomass energy: the scale of the potential resource, Trends Ecol. Evol. 23 (2008) 65, https://doi.org/10.1016/j.tree.2007.12.001.
[14] A.R. Milbrandt, D.M. Heimiller, A.D. Perry, C.B. Field, Renewable energy potential on marginal lands in the United States, Renew. Sustain. Energy Rev. 29 (2014) 473–481, https://doi.org/10.1016/j.rser.2013.08.079.
[15] A. Zumkehr, J.E. Campbell, Historical U.S. cropland areas and the potential for bioenergy production on abandoned croplands, Environ. Sci. Technol. 47 (2013) 3840–3847, https://doi.org/10.1021/es3033132.
[16] G.P.P. Robertson, S.K.S.K. Hamilton, B.L.B.L. Barham, B.E.B.E. Dale, R.C.C. Izaurralde, R.D.R.D. Jackson, D.A.D.A. Landis, S.M.S.M. Swinton, K.D.K.D. Thelen, J.M. Tiedje, Cellulosic biofuel contributions to a sustainable energy future: choices and outcomes, Science (80-.) (2017) 356, https://doi.org/10.1126/science.aal2324.
[17] V. Daioglou, J.C. Doelman, B. Wicke, A. Faaij, D.P. van Vuuren, Integrated assessment of biomass supply and demand in climate change mitigation scenarios, Global Environ. Change 54 (2019) 88–101, https://doi.org/10.1016/j.gloenvcha.2018.11.012.
[18] J.L. Field, T.L. Richard, E.A.H. Smithwick, H. Cai, M.S. Laser, D.S. LeBauer, S.P. Long, K. Paustian, Z. Qin, J.J. Sheehan, P. Smith, M.Q. Wang, L.R. Lynd, Robust paths to net greenhouse gas mitigation and negative emissions via advanced biofuels, Proc. Natl. Acad. Sci. U. S. A 117 (2020) 21968–21977, https://doi.org/10.1073/pnas.1920877117.
[19] Y. Yang, D. Tilman, C. Lehman, J.J. Trost, Sustainable intensification of high-diversity biomass production for optimal biofuel benefits, Nat. Sustain. 1 (2018) 686–692, https://doi.org/10.1038/s41893-018-0166-1.
[20] B.P. Werling, T.L. Dickson, R. Isaacs, H. Gaines, C. Gratton, K.L. Gross, H. Liere, C.M. Malmstrom, T.D. Meehan, L. Ruan, B.A. Robertson, G.P. Robertson, T.M. Schmidt, A.C. Schrotenboer, T.K. Teal, J.K. Wilson, D.A. Landis, Perennial grasslands enhance biodiversity and multiple ecosystem services in bioenergy landscapes, Proc. Natl. Acad. Sci. U. S. A 111 (2014) 1652–1657, https://doi.org/10.1073/pnas.1309492111.
[21] L. Lai, C. Oh Hong, S. Kumar, S.L. Osborne, R.M. Lehman, V.N. Owens, Soil nitrogen dynamics in switchgrass seeded to a marginal cropland in South Dakota, GCB Bioenergy 10 (2018) 28–38, https://doi.org/10.1111/gcbb.12475.
[22] K.J. Harding, T.E. Twine, A. VanLoocke, J.E. Bagley, J. Hill, Impacts of second-generation biofuel feedstock production in the central U.S. on the hydrologic cycle and global warming mitigation potential, Geophys. Res. Lett. 43 (2016) 10,773–10,781, https://doi.org/10.1002/2016GL069981.
[23] P. Zhu, Q. Zhuang, J. Eva, C. Bernacchi, Importance of biophysical effects on climate warming mitigation potential of biofuel crops over the conterminous United States, GCB Bioenergy 9 (2017) 577–590, https://doi.org/10.1111/gcbb.12370.
[24] Y. Yang, S.E. Hobbie, R.R. Hernandez, J. Fargione, S.M. Grodsky, D. Tilman, Y.-G. Zhu, Y. Luo, T.M. Smith, J.M. Jungers, M. Yang, W.-Q. Chen, Restoring abandoned farmland to mitigate climate change on a full earth, One Earth 3 (2020) 176–186, https://doi.org/10.1016/j.oneear.2020.07.019.
[25] A. Goodrich, T. James, M. Woodhouse, Residential, commercial, and utility scale photovoltaic (PV) System prices in the United States: current drivers and cost-reduction opportunities, Photovolt. Costs U.S. Anal. Prices Trends. (2012) 1–58.
[26] International Renewable Energy Agency IRENA, Future of solar photovoltaic: deployment, investment, technology, grid integration and socio-economic aspects. https://www.irena.org/-/media/Files/IRENA/Agency/Publication/2019/Oct/IRENA_Future_of_wind_2019.pdf, 2019.
[27] T.J. Dijkman, R.M.J. Benders, Comparison of renewable fuels based on their land use using energy densities, Renew. Sustain. Energy Rev. 14 (2010) 3148–3155, https://doi.org/10.1016/j.rser.2010.07.029.
[28] B. Pillot, N. Al-Kurdi, C. Gervet, L. Linguet, An integrated GIS and robust optimization framework for solar PV plant planning scenarios at utility scale, Appl. Energy 260 (2020), 114257, https://doi.org/10.1016/j.apenergy.2019.114257.
[29] E.G. Hertwich, T. Gibon, E.A. Bouman, A. Arvesen, S. Suh, G.A. Heath, J.D. Bergesen, A. Ramirez, M.I. Vega, L. Shi, Integrated life-cycle assessment of electricity-supply scenarios confirms global environmental benefit of low-carbon technologies, Proc. Natl. Acad. Sci. U. S. A 112 (2015) 6277–6282, https://doi.org/10.1073/pnas.1312753111.
[30] K. Calvert, W. Mabee, More solar farms or more bioenergy crops? Mapping and assessing potential land-use conflicts among renewable energy technologies in eastern Ontario, Canada, Appl. Geogr. 56 (2015) 209–221, https://doi.org/10.1016/j.apgeog.2014.11.028.
[31] C. Breyer, D. Bogdanov, A. Gulagi1, A. Aghahosseini, L.S.N.S. Barbosa, O. Koskinen, M. Barasa, U. Caldera, S. Afanasyeva, M. Child, J. Farfan1, P. Vainikka, On the role of solar photovoltaics in global energy transition scenarios, IEEE Trans. Fuzzy Syst. 20 (2017) 727–745, https://doi.org/10.1002/pip.
[32] S. Bontemps, P. Defourny, J. Radoux, E. Van Bogaert, C. Lamarche, F. Achard, P. Mayaux, M. Boettcher, C. Brockmann, G. Kirches, M. Zülkhe, V. Kalogirou, O. Arino, Consistent global land cover maps for climate modeling communities: current achievements of the ESA's land cover CCI, in: ESA Living Planet Symp. 2013, 2013, pp. 9–13. https://ftp.space.dtu.dk/pub/Ioana/papers/s274_2bont.pdf.
[33] G. Fischer, F.O. Nachtergaele, S. Prieler, E. Teixeira, G. Toth, H. van Velthuizen, L. Verelst, D. Wiberg, Global Agro-Ecological Zones (GAEZ): Model Documentation, 2012, pp. 1–179.
[34] E. Scoccimarro, S. Gualdi, A. Bellucci, A. Sanna, P.G. Fogli, E. Manzini, M. Vichi, P. Oddo, A. Navarra, Effects of tropical cyclones on ocean heat transport in a high-resolution coupled general circulation model, J. Clim. 24 (2011) 4368–4384, https://doi.org/10.1175/2011JCLI4104.1.
[35] F. Mavromatakis, G. Makrides, G. Georghiou, A. Pothrakis, Y. Franghiadakis, E. Drakakis, E. Koudoumas, Modeling the photovoltaic potential of a site, Renew. Energy 35 (2010) 1387–1390, https://doi.org/10.1016/j.renene.2009.11.010.
[36] J.R. Oakleaf, C.M. Kennedy, S. Baruch-Mordo, J.S. Gerber, P.C. West, J.A. Johnson, J. Kiesecker, Global development potential indicies for renewable energy, fossil fuels, mining and agriculture sectors, figshare, Sci. Data 6 (2019) 101, https://doi.org/10.1038/s41597-019-0084-8.
[37] J.E. Campbell, D.B. Lobell, R.C. Genova, C.B. Field, The global potential of bioenergy on abandoned agriculture lands, Environ. Sci. Technol. 42 (2008) 5791–5794, https://doi.org/10.1021/es800052w.
[38] X. Cai, X. Zhang, D. Wang, Land availability for biofuel production, Environ. Sci. Technol. 45 (2011) 334, https://doi.org/10.1021/es103338e.
[39] R. Slade, A. Bauen, R. Gross, Global bioenergy resources, Nat. Clim. Change 4 (2014) 99–105, https://doi.org/10.1038/nclimate2097.
[40] T. Beringer, W. Lucht, S. Schaphoff, Bioenergy production potential of global biomass plantations under environmental and agricultural constraints, GCB Bioenergy 3 (2011) 299–312, https://doi.org/10.1111/j.1757-1707.2010.01088.x.
[41] Y. Charabi, A. Gastli, PV site suitability analysis using GIS-based spatial fuzzy multi-criteria evaluation, Renew. Energy 36 (2011) 2554–2561, https://doi.org/10.1016/j.renene.2010.10.037.

[42] F. Kienast, N. Huber, R. Hergert, J. Bolliger, L.S.L.S. Moran, A.M.A.M. Hersperger, Conflicts between decentralized renewable electricity production and landscape services – a spatially-explicit quantitative assessment for Switzerland, Renew. Sustain. Energy Rev. 67 (2017) 397–407, https://doi.org/10.1016/j.rser.2016.09.045.
[43] D. Lingfors, J. Widén, J. Marklund, M. Boork, D. Larsson, Photovoltaics in Swedish agriculture: technical potential, grid integration and profitability, in: ISES Sol. World Congr. 2015, Conf. Proc., 2015, pp. 259–267, https://doi.org/10.18086/swc.2015.07.14.
[44] D. Scordia, S.L. Cosentino, Perennial energy grasses: resilient crops in a changing european agriculture, Agric. For. 9 (2019), https://doi.org/10.3390/agriculture9080169.
[45] R.I. Nazli, V. Tansi, H.H. Öztürk, A. Kusvuran, Miscanthus, switchgrass, giant reed, and bulbous canary grass as potential bioenergy crops in a semi-arid Mediterranean environment, Ind. Crop. Prod. 125 (2018) 9–23, https://doi.org/10.1016/j.indcrop.2018.08.090.
[46] A. Ameen, L. Han, G.H. Xie, Dynamics of soil moisture, pH, organic carbon, and nitrogen under switchgrass cropping in a semiarid sandy wasteland, Commun. Soil Sci. Plant Anal. 50 (2019) 922–933, https://doi.org/10.1080/00103624.2019.1594883.
[47] D. Cooney, H. Kim, L. Quinn, M.S. Lee, J. Guo, S. lin Chen, B. cheng Xu, D.K. Lee, Switchgrass as a bioenergy crop in the Loess Plateau, China: potential lignocellulosic feedstock production and environmental conservation, J. Integr. Agric. 16 (2017) 1211–1226, https://doi.org/10.1016/S2095-3119(16)61587-3.
[48] I. Lewandowski, J.M.O. Scurlock, E. Lindvall, M. Christou, The development and current status of perennial rhizomatous grasses as energy crops in the US and Europe, Biomass Bioenergy 25 (2003) 335–361, https://doi.org/10.1016/S0961-9534(03)00030-8.
[49] I. Lewandowski, J.C. Clifton-Brown, J.M.O. Scurlock, W. Huisman, Miscanthus, European experience with a novel energy crop, Biomass Bioenergy 19 (2000) 209–227, https://doi.org/10.1016/S0961-9534(00)00032-5.
[50] G. Siri-Prieto, M. Bustamante, V. Picasso, O. Ernst, Impact of nitrogen and phosphorous on biomass yield, nitrogen efficiency, and nutrient removal of perennial grasses for bioenergy, Biomass Bioenergy 136 (2020), 105526, https://doi.org/10.1016/j.biombioe.2020.105526.
[51] A. Ameen, J. Liu, L. Han, G.H. Xie, Effects of nitrogen rate and harvest time on biomass yield and nutrient cycling of switchgrass and soil nitrogen balance in a semiarid sandy wasteland, Ind. Crop. Prod. 136 (2019) 1–10, https://doi.org/10.1016/j.indcrop.2019.04.066.
[52] B. Zhang, A. Hastings, J.C. Clifton-Brown, D. Jiang, A.P.C. Faaij, Modeled spatial assessment of biomass productivity and technical potential of Miscanthus × giganteus, Panicum virgatum L., and Jatropha on marginal land in China, GCB Bioenergy 12 (2020) 328–345, https://doi.org/10.1111/gcbb.12673.
[53] D. Hui, C.L. Yu, Q. Deng, E. Kudjo Dzantor, S. Zhou, S. Dennis, R. Sauve, T.L. Johnson, P.A. Fay, W. Shen, Y. Luo, Effects of precipitation changes on switchgrass photosynthesis, growth, and biomass: a mesocosm experiment, PLoS One 13 (2018) 1–18, https://doi.org/10.1371/journal.pone.0192555.
[54] Q. Deng, S. Aras, C.L. Yu, E.K. Dzantor, P.A. Fay, Y. Luo, W. Shen, D. Hui, Effects of precipitation changes on aboveground net primary production and soil respiration in a switchgrass field, Agric. Ecosyst. Environ. 248 (2017) 29–37, https://doi.org/10.1016/j.agee.2017.07.023.
[55] N. Ben Fradj, S. Rozakis, M. Borzęcka, M. Matyka, Miscanthus in the European bio-economy: a network analysis, Ind. Crop. Prod. 148 (2020), https://doi.org/10.1016/j.indcrop.2020.112281.
[56] R. Smith, F.M. Slater, The effects of organic and inorganic fertilizer applications to Miscanthus×giganteus, Arundo donax and Phalaris arundinacea, when grown as energy crops in Wales, UK, GCB Bioenergy (2010), https://doi.org/10.1111/j.1757-1707.2010.01051.x no-no.
[57] S. Usťak, J. Šinko, J. Muñoz, Reed canary grass (Phalaris arundinacea l.) as a promising energy crop, J. Cent. Eur. Agric. 20 (2019) 1143–1168, https://doi.org/10.5513/JCEA01/20.4.2267.
[58] R. Dopazo, D. Vega-Nieva, L. Ortiz, Herbaceous energy crops: reviewing their productivity for bioenergy production, Publ. Internet Http//…. https://www.researchgate.net/publication/228481008%0AHttp://193.146.36.56/ence/publicaciones/Valencia_OC7.3.pdf, 2010, 1-3
[59] A. Laurent, E. Pelzer, C. Loyce, D. Makowski, Ranking yields of energy crops: a meta-analysis using direct and indirect comparisons, Renew. Sustain. Energy Rev. 46 (2015) 41–50, https://doi.org/10.1016/j.rser.2015.02.023.
[60] R.C. Miller, J.B. Zedler, Responses of native and invasive wetland plants to hydroperiod and water depth, Plant Ecol. 167 (2003) 57–69, https://doi.org/10.1023/A:1023918619073.
[61] G. Fischer, H. Van Velthuizen, M. Shah, F. Nachtergaele, Global agro-ecological assessment for agriculture in the 21st Century : methodology and results, analysis, RR-02-02, http://www.iiasa.ac.at/Admin/PUB/Documents/RR-02-002.pdf, 2002, 119.
[62] FAO, Aquamaps. Global spatial database on water and agriculture. http://www.fao.org/nr/water/aquamaps/, 2010.
[63] F.R. Rijsberman, Water scarcity: fact or fiction? Agric. Water Manag. 80 (2006) 5–22, https://doi.org/10.1016/j.agwat.2005.07.001.
[64] J. Liu, H. Yang, S.N. Gosling, M. Kummu, M. Flörke, S. Pfister, N. Hanasaki, Y. Wada, X. Zhang, C. Zheng, J. Alcamo, T. Oki, Water scarcity assessments in the past, present, and future, Earth's Futur. 5 (2017) 545–559, https://doi.org/10.1002/2016EF000518.
[65] A. Brown, M.D. Matlock, A Review of Water Scarcity Indices and Methodologies, 2011. White Pap.
[66] FAO, The State of the World's Land and Water Resources for Food and Agriculture: Managing Systems at Risk, Food and Agriculture Organization of the United Nations, Rome Earthscan, London, 2011.
[67] ECN.TNO., Phyllis2, Database for Biomass and Waste, 2019.
[68] S. Jerez, I. Tobin, R. Vautard, J.P. Montávez, J.M. López-Romero, F. Thais, B. Bartok, O.B. Christensen, A. Colette, M. Déqué, G. Nikulin, S. Kotlarski, E. Van Meijgaard, C. Teichmann, M. Wild, The impact of climate change on photovoltaic power generation in Europe, Nat. Commun. 6 (2015), https://doi.org/10.1038/ncomms10014.
[69] M. Wild, D. Folini, F. Henschel, N. Fischer, B. Müller, Projections of long-term changes in solar radiation based on CMIP5 climate models and their influence on energy yields of photovoltaic systems, Sol. Energy 116 (2015) 12–24, https://doi.org/10.1016/j.solener.2015.03.039.
[70] W. Sawadogo, B.J. Abiodun, E.C. Okogbue, Impacts of global warming on photovoltaic power generation over West Africa, Renew. Energy 151 (2020) 263–277, https://doi.org/10.1016/j.renene.2019.11.032.
[71] H.A. Kazem, M.T. Chaichan, I.M. Al-shezawi, H.S. Al-saidi, H.S. Al-rubkhi, K. Al-sinani, A.H.A. Al-waeli, Effect of humidity on the PV performance in Oman, Asian Trans. Eng. 2 (2014) 29–32.
[72] T. Bhattacharya, A.K. Chakraborty, K. Pal, Effects of ambient temperature and wind speed on performance of monocrystalline solar photovoltaic module in Tripura, India, J. Sol. Energy. 2014 (2014) 1–5, https://doi.org/10.1155/2014/817078.
[73] S. Mekhilef, R. Saidur, M. Kamalisarvestani, Effect of dust, humidity and air velocity on efficiency of photovoltaic cells, Renew. Sustain. Energy Rev. 16 (2012) 2920–2925, https://doi.org/10.1016/j.rser.2012.02.012.
[74] S. Pfenninger, I. Staffell, Long-term patterns of European PV output using 30 years of validated hourly reanalysis and satellite data, Energy 114 (2016) 1251–1265, https://doi.org/10.1016/j.energy.2016.08.060.
[75] J. Müller, D. Folini, M. Wild, S. Pfenninger, CMIP-5 models project photovoltaics are a no-regrets investment in Europe irrespective of climate change, Energy 171 (2019) 135–148, https://doi.org/10.1016/j.energy.2018.12.139.
[76] J.A. Crook, L.A. Jones, P.M. Forster, R. Crook, Climate change impacts on future photovoltaic and concentrated solar power energy output, Energy Environ. Sci. 4 (2011) 3101–3109, https://doi.org/10.1039/c1ee01495a.
[77] D. Thevenard, S. Pelland, Estimating the uncertainty in long-term photovoltaic yield predictions, Sol. Energy 91 (2013) 432–445, https://doi.org/10.1016/j.solener.2011.05.006.
[78] N.H. Reich, B. Mueller, A. Armbruster, W.G.J.H.M. van Sark, K. Kiefer, C. Reise, Performance ratio revisited: is PR>90% realistic? Prog. Photovoltaics Res. Appl. 20 (2012) 1114–1129, https://doi.org/10.1002/pip.
[79] E. Roeckner, G. Bauml, L. Bonaventura, R. Brokopf, M. Esch, M. Giorgetta, S. Hagemann, I. Kirchner, L. Kornblueh, E. Manzini, A. Rhodin, U. Schlese, U. Schulzweida, A. Tompkins, The atmospheric general circulation model ECHAM5 model description, J. Geophys. Res. Atmos. 1 (2003), https://doi.org/10.1029/2010JD014036.
[80] G. Madec, P. Delecluse, Institut pierre simon laplace ocean general circulation model reference manual, Tech. Rep. (1998).
[81] S. Valcke, The OASIS3 coupler: a European climate modelling community software, Geosci, Model Dev 6 (2013) 373–388, https://doi.org/10.5194/gmd-6-373-2013.
[82] A. Sanna, P. Lionello, S. Gualdi, Coupled atmosphere ocean climate model simulations in the Mediterranean region: effect of a high-resolution marine model on cyclones and precipitation, Nat. Hazards Earth Syst. Sci. 13 (2013) 1567–1577, https://doi.org/10.5194/nhess-13-1567-2013.
[83] E. Bucchignani, A.L. Zollo, L. Cattaneo, M. Montesarchio, P. Mercogliano, Extreme weather events over China: assessment of COSMO-CLM simulations and future scenarios, Int. J. Climatol. 37 (2017) 1578–1594, https://doi.org/10.1002/joc.4798.
[84] Y. Zheng, J. Han, Y. Huang, S.R. Fassnacht, S. Xie, E. Lv, M. Chen, Vegetation response to climate conditions based on NDVI simulations using stepwise cluster analysis for the Three-River Headwaters region of China, Ecol. Indicat. 92 (2018) 18–29, https://doi.org/10.1016/j.ecolind.2017.06.040.
[85] M.J. Alizadeh, T. Alinejad-Tabrizi, M.R. Kavianpour, S. Shamshirband, Projection of spatiotemporal variability of wave power in the Persian Gulf by the end of 21st century: GCM and CORDEX ensemble, J. Clean. Prod. 256 (2020), https://doi.org/10.1016/j.jclepro.2020.120400.
[86] I.F. Abdin, Y.P. Fang, E. Zio, A modeling and optimization framework for power systems design with operational flexibility and resilience against extreme heat waves and drought events, Renew. Sustain. Energy Rev. 112 (2019) 706–719, https://doi.org/10.1016/j.rser.2019.06.006.
[87] J.C. Pérez, A. González, J.P. Díaz, F.J. Expósito, J. Felipe, Climate change impact on future photovoltaic resource potential in an orographically complex archipelago, the Canary Islands, Renew. Energy 133 (2019) 749–759, https://doi.org/10.1016/j.renene.2018.10.077.
[88] B. François, B. Hingray, M. Borga, D. Zoccatelli, C. Brown, J.D. Creutin, Impact of climate change on combined solar and run-of-river power in Northern Italy, Energies 11 (2018) 1–22, https://doi.org/10.3390/en11020290.
[89] A. Bichet, B. Hingray, G. Evin, A. Diedhiou, C.M.F. Kebe, S. Anquetin, Potential impact of climate change on solar resource in Africa for photovoltaic energy: analyses from CORDEX-Africa climate experiments, Environ. Res. Lett. 14 (2019), https://doi.org/10.1088/1748-9326/ab500a.
[90] R. Chenni, M. Makhlouf, T. Kerbache, A. Bouzid, A detailed modeling method

for photovoltaic cells, Energy 32 (2007) 1724–1730, https://doi.org/10.1016/j.energy.2006.12.006.
[91] J.K. Tonui, Y. Tripanagnostopoulos, Performance improvement of PV/T solar collectors with natural air flow operation, Sol. Energy 82 (2008) 1–12, https://doi.org/10.1016/j.solener.2007.06.004.
[92] P. Ruiz, W. Nijs, D. Tarvydas, A. Sgobbi, A. Zucker, R. Pilli, R. Jonsson, A. Camia, C. Thiel, C. Hoyer-Klick, F. Dalla Longa, T. Kober, J. Badger, P. Volker, B.S. Elbersen, A. Brosowski, D. Thrän, ENSPRESO - an open, EU-28 wide, transparent and coherent database of wind, solar and biomass energy potentials, Energy Strateg. Rev. 26 (2019), 100379, https://doi.org/10.1016/j.esr.2019.100379.
[93] J. Malczewski, C. Rinner, Multicriteria decision analysis in geographic information science. https://doi.org/10.1007/978-3-540-74757-4, 2015.
[94] S. Dunnett, A. Sorichetta, G. Taylor, F. Eigenbrod, Harmonised global datasets of wind and solar farm locations and power, Sci. Data 7 (2020) 1–12, https://doi.org/10.1038/s41597-020-0469-8.
[95] T.L. Saaty, How to make a decision: the analytic hierarchy process, Eur. J. Oper. Res. 48 (1990) 9–26, https://doi.org/10.1016/0377-2217(90)90057-I.
[96] ESRi, ArcGIS Desktop 10.7: ArcMap Functionality Matrix, 2019.
[97] H. Yin, A. B Jr., J. Buchner, D. Helmers, B.G. Iuliano, N.E. Kimambo, K.E. Lewińska, E. Razenkova, A. Rizayeva, N. Rogova, S.A. Spawn, Y.H. Xie, V.R. C, Monitoring cropland abandonment with Landsat time series, in review, Remote Sens. Environ. 246 (2020), https://doi.org/10.1016/j.rse.2020.111873.
[98] G.I. Díaz, L. Nahuelhual, C. Echeverría, S. Marín, Drivers of land abandonment in Southern Chile and implications for landscape planning, Landsc. Urban Plann. 99 (2011) 207–217, https://doi.org/10.1016/j.landurbplan.2010.11.005.
[99] P. Meyfroidt, F. Schierhorn, A.V. Prishchepov, D. Müller, T. Kuemmerle, Drivers, constraints and trade-offs associated with recultivating abandoned cropland in Russia, Ukraine and Kazakhstan, Global Environ. Change 37 (2016) 1–15, https://doi.org/10.1016/j.gloenvcha.2016.01.003.
[100] J. Kamp, A. Reinhard, M. Frenzel, S. Kämpfer, J. Trappe, N. Hölzel, Farmland bird responses to land abandonment in Western Siberia, Agric. Ecosyst. Environ. 268 (2018) 61–69, https://doi.org/10.1016/j.agee.2018.09.009.
[101] C. Quéré, R. Andrew, P. Friedlingstein, S. Sitch, J. Hauck, J. Pongratz, P. Pickers, J. Ivar Korsbakken, G. Peters, J. Canadell, A. Arneth, V. Arora, L. Barbero, A. Bastos, L. Bopp, P. Ciais, L. Chini, P. Ciais, S. Doney, T. Gkritzalis, D. Goll, I. Harris, V. Haverd, F. Hoffman, M. Hoppema, R. Houghton, G. Hurtt, T. Ilyina, A. Jain, T. Johannessen, C. Jones, E. Kato, R. Keeling, K. Klein Goldewijk, P. Landschützer, N. Lefèvre, S. Lienert, Z. Liu, D. Lombardozzi, N. Metzl, D. Munro, J. Nabel, S.I. Nakaoka, C. Neill, A. Olsen, T. Ono, P. Patra, A. Peregon, W. Peters, P. Peylin, B. Pfeil, D. Pierrot, B. Poulter, G. Rehder, L. Resplandy, E. Robertson, M. Rocher, C. Rödenbeck, U. Schuster, I. Skjelvan, R. Séférian, I. Skjelvan, T. Steinhoff, A. Sutton, P. Tans, H. Tian, B. Tilbrook, F. Tubiello, I. Van Der Laan-Luijkx, G. Van Der Werf, N. Viovy, A. Walker, A. Wiltshire, R. Wright, S. Zaehle, B. Zheng, Global carbon budget 2018, Earth Syst. Sci. Data 10 (2018), https://doi.org/10.5194/essd-10-2141-2018.
[102] S.A. Spawn, C.C. Sullivan, T.J. Lark, H.K. Gibbs, Harmonized global maps of above and belowground biomass carbon density in the year 2010, Sci. Data 7 (2020) 1–22, https://doi.org/10.1038/s41597-020-0444-4.
[103] ESA, Land cover CCI: product user guide version 2.0 [Online], https://maps.elie.ucl.ac.be/CCI/viewer/download/ESACCI-LC-Ph2-PUGv2_2.0.pdf, 2017.
[104] Y. Yang, P. Xiao, X. Feng, H. Li, Accuracy assessment of seven global land cover datasets over China, ISPRS J. Photogrammetry Remote Sens. 125 (2017) 156–173, https://doi.org/10.1016/j.isprsjprs.2017.01.016.
[105] A. Pérez-Hoyos, F. Rembold, H. Kerdiles, J. Gallego, Comparison of global land cover datasets for cropland monitoring, Rem. Sens. 9 (2017), https://doi.org/10.3390/rs9111118.
[106] L. Liang, Q. Liu, G. Liu, H. Li, C. Huang, Accuracy evaluation and consistency analysis of four global land cover products in the arctic region, Rem. Sens. 11 (2019), https://doi.org/10.3390/rs11121396.
[107] W. Hou, X. Hou, Data fusion and accuracy analysis of multi-source land use/land cover datasets along coastal areas of the Maritime Silk Road, ISPRS Int. J. Geo-Inf. 8 (2019), https://doi.org/10.3390/ijgi8120557.
[108] X. Liu, L. Yu, W. Li, D. Peng, L. Zhong, L. Li, Q. Xin, H. Lu, C. Yu, P. Gong, Comparison of country-level cropland areas between ESA-CCI land cover maps and FAOSTAT data, Int. J. Rem. Sens. 39 (2018) 6631–6645, https://doi.org/10.1080/01431161.2018.1465613.
[109] G. Duveiller, J. Hooker, A. Cescatti, The mark of vegetation change on Earth's surface energy balance, Nat. Commun. 9 (2018), https://doi.org/10.1038/s41467-017-02810-8.
[110] B. Huang, X. Hu, G.A. Fuglstad, X. Zhou, W. Zhao, F. Cherubini, Predominant regional biophysical cooling from recent land cover changes in Europe, Nat. Commun. 11 (2020) 1–13, https://doi.org/10.1038/s41467-020-14890-0.
[111] C. Folberth, N. Khabarov, J. Balkovič, R. Skalský, P. Visconti, P. Ciais, I.A. Janssens, J. Peñuelas, M. Obersteiner, The global cropland-sparing potential of high-yield farming, Nat. Sustain. 3 (2020) 281–289, https://doi.org/10.1038/s41893-020-0505-x.
[112] J. van Vliet, Direct and indirect loss of natural area from urban expansion, Nat. Sustain. 2 (2019) 755–763, https://doi.org/10.1038/s41893-019-0340-0.
[113] X. Hu, B. Huang, F. Verones, O. Cavalett, F. Cherubini, Overview of recent land cover changes in the biodiversity hotspots. https://doi.org/10.31223/osf.io/4rwda, 2020, 1-7.
[114] S. Kang, S. Selosse, N. Maïzi, Contribution of global GHG reduction pledges to bioenergy expansion, Biomass Bioenergy 111 (2018) 142–153, https://doi.org/10.1016/j.biombioe.2017.05.017.
[115] M.D. Staples, R. Malina, P. Suresh, J.I. Hileman, S.R.H. Barrett, Aviation CO2 emissions reductions from the use of alternative jet fuels, Energy Pol. 114 (2018) 342–354, https://doi.org/10.1016/j.enpol.2017.12.007.
[116] N. Deng, P. Grassini, H. Yang, J. Huang, K.G. Cassman, S. Peng, Closing yield gaps for rice self-sufficiency in China, Nat. Commun. 10 (2019) 1–9, https://doi.org/10.1038/s41467-019-09447-9.
[117] K.F. Davis, M.C. Rulli, A. Seveso, P. D'Odorico, Increased food production and reduced water use through optimized crop distribution, Nat. Geosci. 10 (2017) 919–924, https://doi.org/10.1038/s41561-017-0004-5.
[118] M.D. Staples, H. Olcay, R. Malina, P. Trivedi, M.N. Pearlson, K. Strzepek, S.V. Paltsev, C. Wollersheim, S.R.H. Barrett, Water consumption footprint and land requirements of large-scale alternative diesel and jet fuel production, Environ. Sci. Technol. 47 (2013) 12557–12565, https://doi.org/10.1021/es4030782.
[119] M.Z. Jacobson, Review of solutions to global warming, air pollution, and energy security, Energy Environ. Sci. 2 (2009) 148–173, https://doi.org/10.1039/b809990c.
[120] V.V. Tyagi, N.A.A. Rahim, N.A.A. Rahim, J.A.L. Selvaraj, Progress in solar PV technology: research and achievement, Renew. Sustain. Energy Rev. 20 (2013) 443–461, https://doi.org/10.1016/j.rser.2012.09.028.
[121] U. Desideri, F. Zepparelli, V. Morettini, E. Garroni, Comparative analysis of concentrating solar power and photovoltaic technologies: technical and environmental evaluations, Appl. Energy 102 (2013) 765–784, https://doi.org/10.1016/j.apenergy.2012.08.033.
[122] C. Xu, T.A. Kohler, T.M. Lenton, J.C. Svenning, M. Scheffer, Future of the human climate niche, Proc. Natl. Acad. Sci. U. S. A 117 (2020), https://doi.org/10.1073/pnas.1910114117.
[123] S. Levis, A. Badger, B. Drewniak, C. Nevison, X. Ren, CLMcrop yields and water requirements: avoided impacts by choosing RCP 4.5 over 8.5, Climatic Change 146 (2018) 501–515, https://doi.org/10.1007/s10584-016-1654-9.
[124] T.J. Troy, C. Kipgen, I. Pal, The impact of climate extremes and irrigation on US crop yields, Environ. Res. Lett. 10 (2015), https://doi.org/10.1088/1748-9326/10/5/054013.
[125] B. Schauberger, S. Archontoulis, A. Arneth, J. Balkovic, P. Ciais, D. Deryng, J. Elliott, C. Folberth, N. Khabarov, C. Müller, T.A.M. Pugh, S. Rolinski, S. Schaphoff, E. Schmid, X. Wang, W. Schlenker, K. Frieler, Consistent negative response of US crops to high temperatures in observations and crop models, Nat. Commun. 8 (2017), https://doi.org/10.1038/ncomms13931.
[126] E.H. Adeh, S.P. Good, M. Calaf, C.W. Higgins, Solar PV power potential is greatest over croplands, Sci. Rep. 9 (2019) 1–6, https://doi.org/10.1038/s41598-019-47803-3.
[127] D.E.H.J. Gernaat, P.W. Bogaart, D.P.V. Vuuren, H. Biemans, R. Niessink, High-resolution assessment of global technical and economic hydropower potential, Nat. Energy 2 (2017) 821–828, https://doi.org/10.1038/s41560-017-0006-y.